Self-Assembled Nano-Checkerboard Thin Films Studied by Reciprocal Space Mapping at CHESS

S.M. O'Malley[1], P. Bonanno[1], K.H. Ahn[1], A.A. Sirenko[1], A. Kazimirov[2], S. Park[3], Y. Horibe[3], and S.-W. Cheong[3]

[1]*Dept. of Physics, New Jersey Institute of Technology*
[2]*Cornell High Energy Synchrotron Source, Cornell University*
[3]*Rutgers Center for Emergent Materials and Dept. of Physics and Astronomy, Rutgers University*

Material systems that can self-assemble into nano-structures are of great interest because of their ability to form compositionally and spatially distinct regions otherwise unattainable through traditional materials processing techniques like optical or electron beam lithography. The spinel oxide $ZnMnGaO_4$ (ZMGO) was recently discovered to undergo a self-assembly process during slow annealing of bulk samples[1]. Nano-structure formation in ZMGO occurs during the annealing process and is driven by a combination of spinoidal decomposition between Jahn-Teller-active and -inactive ions and spatial separation through diffusion processes[1-4]. The bulk ZMGO crystals end up being comprised of Mn-rich and Mn-poor nanorods forming a checkerboard (CB) pattern within the *a*-*b* plane that is accompanied by a herringbone (HB) arrangement along the *c*-direction.

For the purpose of future device fabrication, nano-scale structures should be available in thin-film form, whereby, the material properties can be enhanced through the overall reduction in volume and by the strain associated with heteroepitaxial growth. Our ZMGO thin films were grown using pulsed laser deposition by the research team at Rutgers University Center for Emergent Materials[5]. The target material was a homogenous high-temperature quenched form of ZMGO, with a tetragonal lattice (a = 0.82 nm, c = 0.87 nm); the substrate was single crystal cubic MgO (0 0 1) with lattice constant a = 0.4212 nm. Transmission electron microscopy (TEM) revealed that the films indeed contain an in-plane CB pattern with suppression of the out-plane HB formation. The typical nanorod length in the epitaxial films increased to 4×4×700 nm^3 compared with 4×4×70 nm^3 for the bulk material. Portions of this work have been published in References [5,6].

Experiment

To determine structural parameters and strain-accommodating distortions for the CB films we utilized reciprocal space mapping at the A2 x-ray diffraction (XRD) beamline of Cornell High Energy Synchrotron Source (CHESS). The incident x-ray beam was conditioned using a double-bounce Si (1 1 1) monochromator passing photons with an energy of 10.531 keV (λ=1.1775 Å). High angular resolution was achieved by using a single-bounce Si (1 1 1) analyzer crystal. Reciprocal space mapping of the ZMGO checkerboard structures were measured for several symmetric and asymmetric reflections: (0 0 2), (−2 0 2), (−2 −2 2), (0 0 4), (0 4 4), (−2 2 6). The Miller index L corresponds to the film growth direction, while H and K represent the in-plane parameters of the structure. The integer values of H, K, and L correspond to reciprocal lattice points (RLP) of a cubic spinel structure with lattice parameter a_S = 0.8424 nm (*i.e.*, twice the corresponding value for the cubic MgO substrate).

Results

Figure 1, depicts a 3-dimenional construct of H–K, H–L, and K–L cross sectional maps measured around the asymmetric (0 4 4) RLP. The map is dominated by several peaks, associated with different phases within the CB film. The four broad peaks labeled α, ß, γ, and δ correspond to two conversely rotated tetragonal (ß and γ) and two perpendicularly-oriented orthorhombic (α and δ) phases, respectively. The four diagonal peaks (ρ, σ, τ, υ) correspond to the structural distortions originating from domain boundaries between checkerboard phases. The average in-plane lattice parameter of the two rotated tetragonal phases are lattice-matched to the substrate, *i.e.* the tetragonal phase is elastically strained with in-plane lattice constant of a_{tet} = 0.841 nm. These tetragonal phases of the ß and γ peaks are rotated by ±2.55° around the (0 0 L) reciprocal lattice vector. The orthorhombic phases α and δ have short and long in-plane lattice parameters a_{otho} = 0.814 nm and b_{otho} = 0.898 nm, respectively, and are therefore inelastically strained. The diffraction peak intensity of the structural phases were integrated over their volume in reciprocal space in order to determine the prevalence of each phase within the film. The total intensity of the four α, ß, γ, and δ peaks is ~6 times that of the central tetragonal phase (*A*). This

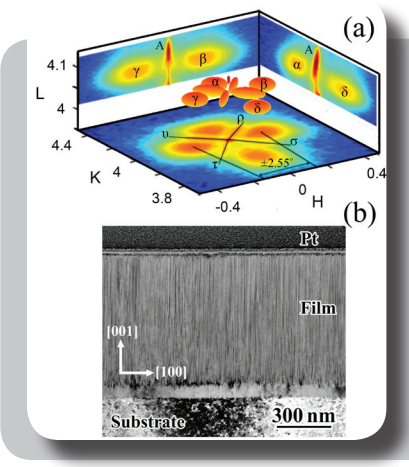

Fig. 1: (a) The H–K, H–L, and K–L cross-sectional RSM measured around the asymmetric (0 4 4) reflection, with L = 4.08. The α and δ peaks are orthorhombic phases, while the ß and γ peaks are rotated tetragonal phases associated with the CB structure. The elastically strained tetragonal phase is labeled *A*. Signal originating from domain boundaries, highlighted by the radial lines emanating from the central (0 4 4) RLP, are labeled ρ, σ, τ and υ. The central figure is a 3D reconstruction of experimentally determined FWHMs of the corresponding peaks. Reprinted figure with permission from Reference [6]. Copyright (2008) by the American Physical Society. (b) TEM image of the CB film on MgO substrate.

ratio is consistent with results from TEM images, and supports the assumption that this central peak *A* originates from the elastically strained transition layer between the CB layer and MgO substrate.

Discussion

The CB epilayer therefore, contains four structurally different spinel phases: two conversely rotated tetragonal (Mn-poor, JT inactive) and two orthogonally oriented orthorhombic (Mn-rich, JT-active) phases. Each of the 4×4×750 nm^3 nano-rod domains is formed by one of these four distorted unit cell phases as depicted in **Figure 2(a)**. The dashed lines in **Fig. 2(b)** define the CB super-cell, which through translational operations can produce the entire CB film. The orthorhombic and rotated tetragonal phases are separated by domain boundaries (DB) closely aligned along the <1 1 0> and <1 −1 0> directions. These domain walls should accommodate structural distortions between the α, ß, γ, and δ phases and provide a means for their coherent growth along both the film growth direction and in the *a*–*b* plane. Comparing the in-plane domain size (4×4 nm^2) and the in-plane footprint of the spinel lattice (~ 0.8×0.8 nm^2), we determined that the fraction of distorted unit cells at the DB is significant (~30%) in comparison to the number of undistorted cells within each phase, see **Fig. 2(b)**. Hence, these DBs should also produce a significant contribution to the total diffraction picture as illustrated by the prominent diagonal streak in the (0 4 4) RSM.

The symmetry of the lattice distortions at the domain boundaries of the CB pattern can be described in terms of distortions with respect to a 2D square lattice with monoatomic basis[7]. These distortions can be represented as a linear combination of e_3, r, and two other modes, either t_+ and s_+ or t_- and s_-. For example, distortions at the interface between the γ and δ domains, as illustrated in **Fig. 3**, can be characterized by a combination of the $-e_3 + r + t_+ + s_+$ distortion modes with amplitudes of $e_3 = -\varepsilon/2$, $r = \varepsilon/2$, $t_+ = \varepsilon/2$, and $s_+ = \varepsilon/2$.

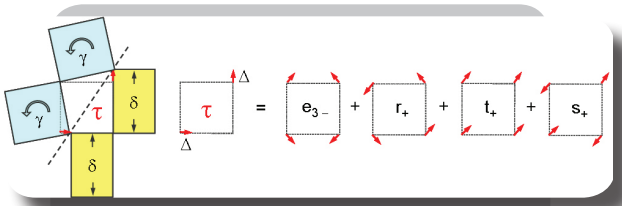

Fig. 3: Representation of the linear combination of distortion modes at the domain boundary τ. Squares γ and rectangles δ correspond to the rotated tetragonal and orthorhombic lattices, respectively.

The role that the substrate plays in establishing and stabilizing the CB structure should not be overlooked as its influence can be seen in a number of aspects, *e.g.*, the suppression of the out-plane herringbone formation. In the case of ZMGO thin films grown on $MgAl_2O_3$ substrates ($a_S = 0.8083$ nm) the film is under a compressive strain in contrast to the previously described case of growth on MgO, where the film is under stabilizing tensile strain. Results from TEM and RSM reveal that ZMGO samples grown on $MgAl_2O_3$ have regressed back to forming the out-plane herringbone structure. Evidence of the HB structure can be seen in **Fig. 4(a)**, where the signal originates from a pair of tilted inelastic tetragonal phases and two tilted elastically strained tetragonal phases, which appears around the symmetric (0 0 4) reflection. The elastic tetragonal phases are accompanied by rotations around K and H axes by about ±0.9 deg and the inelastic tetragonal phases are tilted by about ±1.4 deg. The long diagonal strikes originate form the canted nanorod interfaces, that is similar to the data shown in **Fig. 1** for the CB films.

Conclusion

The use of synchrotron radiation-based reciprocal space mapping (RSM) was paramount in investigating the complex structural properties of epitaxially grown $ZnMnGaO_4$ thin films on single crystal MgO (0 0 1) substrates. The $ZnMnGaO_4$ films consist of a self-assembled CB structure of highly aligned and regularly spaced vertical nano-rods. Reciprocal space mapping revealed the strain-accommodating interaction between the phases of the CB structure through lowering of the volume strain energy, while maintaining long-range commensurability of the structure with the MgO substrate. Such a planar CB surface could be utilized as a template for the subsequent growth of ferromagnetic material and the possible construction of high-density magnetic recording devices. Work at NJIT and Rutgers was supported by the DE-FG02-07ER46382 and the NSF-DMR-0546985.

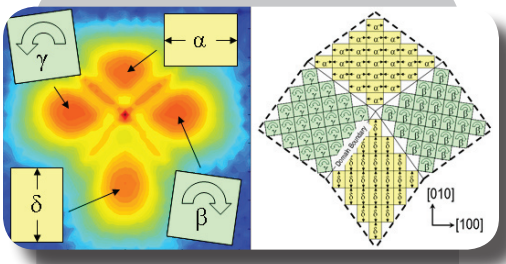

Fig. 2: (a) Illustration of the four structural unit cell phases present with the CB layer with arrows pointing to the appearance with the asymmetric (0 4 4) RSM. (b) Illustration of the CB arrangement of tetragonal and orthorhombic domains with DB along the <1 1 0> and <1 -1 0> directions. The dashed lines define the CB super-cell (SC) by which translational operations can repeat the entire CB film.

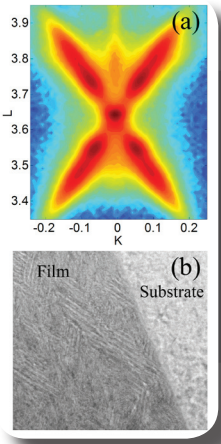

Fig. 4: (a) cross-sectional H-L RSM taken of the symmetric (004) reflection from ZMGO thin film grown on $MgAl_2O_3$. (b) TEM image showing HB structure.

References

1. S. Yeo, Y. Horibe, S. Mori, C.M. Tseng, C.H. Chen, A.G. Khachaturyan, C.L. Zhang, and S-W. Cheong; App. Phys. Lett. **89**, 233120 (2006)
2. C.L. Zhang, S. Yeo, Y. Horibe, Y.J. Choi, S. Guha, M. Croft, S-W. Cheong, and S. Mori; Appl. Phys. Lett. **90**, 133123 (2007)
3. Y. Ni, Y. M. Jin, and A. G. Khachaturyan; Acta Mat. **55**, 4903 (2007)
4. M.A. Ivanov, N. K. Tkachev, and A. Ya. Fishman; Low Temp. Phys. **25**, 459 (1999)
5. S. Park, Y. Horibe, T. Asada, L.S. Wielunski, N. Lee, P. L. Bonanno, S.M. O'Malley, A.A. Sirenko, A. Kazimirov, M. Tanimura, T. Gustafsson, and S-W. Cheong; Nano Lett. **8**, 720 (2008)
6. S.M. O'Malley, P.L. Bonanno, K.H. Ahn, A.A. Sirenko, A. Kazimirov, M. Tanimura, T. Asada, S. Park, Y. Horibe, and S-W. Cheong; Phys. Rev. B **78**, 165425 (2008), http://link.aps.org/abstract/PRB/v78/p165424
7. K.H. Ahn, T. Lookman, A. Saxena, and A. R. Bishop; Phys. Rev. B **68**, 092101 (2003)